Indian Journal of Pure & Applied Physics
Vol. 64, May 2026, pp. 566-578
DOI: 10.56042/ijpap.v65i5.28566

Plasmonic Enhancement in Bimetallic Ag/Au–GST–BP Multilayer SPR Structures for VOC Detection

Vivek Saxena[a], Parita Jain[b], Saibal Manna[a], Varun Gupta[c], Amaresh Gantayet[d], Navneet Kumar[e] & Nishant Kumar[f*]

[a]Department of Electrical & Computer Engineering, ABES Engineering College, Ghaziabad 201 009, India
[b]Department of Computer Science and Engineering, Krishna Institute of Engineering & Technology, Ghaziabad 201 007, India
[c]Department of Electronics and Communication Engineering, National Institute of Technology, Ravangla 737 139, India
[d]Department of Electrical & Electronics Engineering, Siksha O Anusandhan, deemed to be University, Bhubaneswar 751 030, India
[e]Department of Electrical Engineering, Rajkiya Engineering College, Bijnor 246 725, India
[f]Department of Electrical Engineering, B K Birla Institute of Engineering & Technology, Pilani 333 031, India

Received: 11th February 2026; accepted: 5th March 2026

This study presents a bimetallic surface plasmon resonance (SPR) sensor for the non-invasive detection of volatile organic compounds (VOCs) in human breath, targeting early diagnosis of liver and pulmonary diseases. The proposed multilayer structure consists of a NaF prism, Ag/Au bilayer, $Ge_2Sb_2Te_5$ (GST) phase-change material, black phosphorus (BP) layers, and a sensing medium. Finite element simulations using COMSOL Multiphysics were conducted to evaluate angular reflectance characteristics and optimize layer thicknesses and BP stacking. Sensor performance was assessed through resonance angle shifts corresponding to variations in VOC concentration. The optimized configuration, comprising amorphous GST and 18 BP layers, demonstrated superior sensitivity due to enhanced electromagnetic interaction at the sensing interface. The sensor achieved refractive index sensitivities of 1500 RIU^{-1} for lung disease biomarkers and 163.630 RIU^{-1} for liver-related biomarkers. These results highlight the potential of the proposed SPR design for accurate, breath-based biomedical diagnostics.

Keywords: Surface plasmon resonance sensor, Black phosphorus, Phase-change material, Breath-based biomedical diagnostics

1 Introduction

Over the past few decades, biosensors have gained considerable attention as a key research focus within the domain of sensing technologies, with particular emphasis on optical SPR methodologies. This increasing interest is largely attributed to the unique ability of biosensors to enable label-free, real-time detection of a wide range of biomolecules[1, 2]. Their versatile functionality has facilitated significant advancements across multiple fields, including chemical sensing, liquid level detection, gas monitoring, and clinical diagnostic applications[3].

The operational foundation of SPR-based sensor systems lies in the excitation of SPWs, (Surface Plasmon Waves)which are generated by inducing a TM (Transverse Magnetic)polarized electromagnetic wave at the interface of a metallic and dielectric medium. Typically, this involves coating a thin metal film often Au or Ag onto a prism surface. When light impinges upon this metal-dielectric interface under appropriate conditions, it interacts with the interface-bound elements, leading to the excitation of SPs (Surface plasmons). For optimal SPR response, it is essential to match the propagation constant of the incident light with that of the SPs, ensuring efficient energy transfer and resonance conditions[4].

The resonance angle denotes the precise angle of incidence at which SPR is initiated. At this specific incidence angle, the coupling between the incoming electromagnetic wave and the metal dielectric boundary facilitates the excitation of surface plasmon modes. This phenomenon significantly enhances the sensitivity of the SPR sensor to even minor variations in the RI (Refractive Index) of the analyte in proximity to the sensor surface. This phenomenon is typically characterized by a pronounced reduction in the intensity of reflected light, commonly identified as the resonance dip.

*Corresponding author: E-mail:nishant.kumar@bkbiet.ac.in

The RI of the surrounding medium uniquely determines the resonance condition, illustrated by the reflectance intensity curve. This sensitivity to RI changes is a key advantage of SPR-based sensing, allowing for the detection of a broad spectrum of analytes with high precision.

Among the various experimental configurations, the Kretschmann configuration is most commonly employed to realize SPR, primarily due to its structural simplicity and ease of fabrication[5, 6]. In this configuration, the selection of the metal layer is of paramount importance, as it governs the excitation and propagation characteristics of the SPW. This, in turn, critically influences the overall performance parameters of the sensor, particularly its sensitivity and operational efficiency.

For plasmonic applications, Au and Ag are generally favored over metals due to their exceptional capacity to sustain pronounced localized SPR within the visible and near-infrared wavelength ranges. This characteristic significantly contributes to the enhanced sensitivity and efficiency of SPR sensors.

In the field of plasmonic sensors, Ag is widely regarded as the most effective material for achieving maximum field enhancement due to its exceptionally low electrical resistivity and minimal optical losses. Although Au exhibits slightly higher optical losses than Ag, it remains highly efficient, with relatively low energy dissipation. Cu, despite being a good electrical conductor, suffers from increased optical losses, limiting its suitability for plasmonic applications[7]. Al demonstrates pronounced plasmonic activity in the ultraviolet spectral region due to its favorable electronic properties. However, its practical applicability is significantly limited by its high susceptibility to surface oxidation and pronounced intrinsic losses, particularly across the visible and infrared regions of the electromagnetic spectrum. In contrast, Pt is recognized for its excellent chemical inertness and long-term environmental stability. Nevertheless, it exhibits inherently weak plasmonic characteristics within the visible and infrared domains, thereby restricting its effectiveness in applications requiring strong localized surface plasmon resonances in these spectral ranges.

To harness the complementary advantages of both Ag and Au, a bi-metallic Ag-Au architecture has been proposed and employed. Sensitivity enhancements can be further achieved through the integration of a thin film of GST, a phase-change material known for its remarkable optical tunability[8]. GST can reversibly switch between amorphous and crystalline phases, each exhibiting distinct and advantageous optical and electrical characteristics[9]. Notably, this phase transition is accompanied by a pronounced variation in the RI, which is critical for tuning and enhancing plasmonic responses[10]. Furthermore, GST demonstrates strong light matter interaction and efficient light absorption across various wavelengths, reinforcing its potential in active plasmonic sensor designs[11].

Over the past few decades, 2D nanomaterials have emerged as promising candidates in the advancement of SPR technologies, owing to their unique physicochemical properties and broad applicability across diverse research fields. Since the groundbreaking isolation of graphene in 2004, extensive research has been conducted on a range of 2D materials, including BP, MXene, WS_2, MoS_2, and others. These materials exhibit an exceptionally high surface-to-volume ratio, attributed to their atomically thin layered structures[12-15].

Among these, BP has recently attracted substantial attention, particularly for its potential in gas sensing applications[16]. For instance, the authors reported an SPR sensor exhibiting a sensitivity of 218 degrees per RI unit (Deg/RIU) at an excitation wavelength of 633 nm. In a distinct theoretical investigation, the researchers[17] proposed an SPR-based sensor architecture incorporating a BP/MXene heterostructure, aimed at detecting glucose in urine and hemoglobin in blood specimens. Similarly, the authors[12] introduced an improved SPR sensor design integrating Au and BP, highlighting the pivotal contribution of BP in enhancing the sensitivity and performance of gas sensing applications.

Furthermore, the study conducted by[18] introduced a SPR sensing architecture specifically tailored for the detection of NO_2 gas. The results underscored the critical role of BP in significantly improving the sensor's selectivity for NO_2, particularly under conditions where other oxygen-containing molecular species are present. This enhancement is attributed to BP’s unique physicochemical properties, which facilitate stronger and more specific interactions with nitrogen dioxide, thereby minimizing cross-sensitivity and improving detection reliability in complex gas mixtures.

To facilitate the detection of blood plasma, the authors introduced a SPR sensor employing BP as a

sensing material. Their design incorporated four distinct metallic layers. The study revealed that the Cu/BP combination yields enhanced sensitivity, whereas the Ag/BP configuration offers superior detection accuracy and a higher quality factor[19].

Building on their earlier findings, the research team further demonstrated that the strategic integration of 2D nanomaterials with MXene layers can markedly intensify electromagnetic-wave attenuation at the metal dielectric boundary. Leveraging this improvement, they engineered a multilayer SPR platform for uric-acid sensing. The optimised architecture composed of a silver plasmonic layer capped sequentially with WS_2, graphene, and MXene provides superior field confinement and enhanced analyte interaction. As a result, the sensor achieved an impressive sensitivity of 273.53 ° per refractive-index unit, representing a substantial advance over conventional SPR configurations[20].

Further optimizing their design, the researchers employed a BK7 prism, a bimetallic Ag/Au film, and 2D materials including WS_2 and MXene. The sensor exhibited effective performance at a wavelength of 633 nm and operated within a RI range of 1.33 to 1.335 RIU, demonstrating its potential in biomolecular and analyte detection[21].

The latest advancements in biosensing technologies facilitated by metasurfaces highlighted the significant impact of metasurfaces in areas such as medical diagnostics, biomolecular detection, and disease surveillance. The unique capability of metasurfaces to localize electromagnetic fields and modulate optical resonances positions them as highly promising tools for applications including cancer diagnosis and glucose monitoring[22].

A high-performance chemical SPR sensor consisting of a ZnO–Silicon Ag multilayer stack integrated on a BaF_2 prism is proposed. This structure delivered significant sensitivity and figure of merit across a broad range of sensing environments, particularly for refractive indices spanning from[23]1.3264 to 1.36.

In a significant advancement, the researchers proposed a SPR-based gas sensor featuring a multilayered configuration composed of Au, Cu, ZnO, and BP. This carefully engineered structure was designed to enhance the sensor's performance in detecting flammable and toxic gaseous substances. Through systematic analysis, the sensor exhibited remarkable improvements in key performance indicators, including sensitivity, detection accuracy, and FoM, which are critical for reliable gas monitoring. Notably, the sensor demonstrated exceptional responsiveness to NO_2, registering a peak sensitivity of 374.31°/RIU. This value represents a substantial enhancement over traditional gas sensor technologies, underscoring the superior detection capabilities facilitated by the synergistic effects of the multilayer SPR configuration[24].

In recent years, breath analysis has garnered significant attention as a promising diagnostic approach, largely propelled by innovations in nanotechnology and analytical techniques. This method facilitates the identification of various VOCs present in human exhaled breath, thereby offering a non-invasive pathway for the early detection of a range of medical conditions, including liver fibrosis and lung carcinoma[25]. Notably, elevated concentrations of isoprene have been closely associated with liver fibrosis, whereas higher levels of toluene have demonstrated a strong linkage to lung cancer[26-29]. These correlations are well-documented within the domain of medical physics. Consequently, breath analysis holds considerable promise as an early-stage screening tool for hepatic and respiratory diseases, with the potential to contribute to a decline in disease-related mortality rates.

Recent studies further highlight the rapid advancement of SPR technologies. For instance, Fe_3O_4/Ag nanocomposite-based SPR sensors demonstrated enhanced plasmonic activity and low LOD through TMOKE-assisted modulation[30]. A graphene–WS_2–CNT multilayer SPR biosensor achieved a remarkable sensitivity of 400°/RIU for non-invasive glucose monitoring[31], while Sb-incorporated S–Se–Ge chalcogenide glass layers enabled narrow resonance linewidths and high sensitivity up to 160.9°/RIU in Kretschmann-based configurations[32].

This study advances the current state of research by introducing a range of innovative contributions that collectively address the need for sensitive, non-invasive diagnostic methods targeting pulmonary and hepatic disorders. It specifically presents a novel breath-based detection framework that leverages the identification of VOC biomarkers exhaled by patients. To achieve enhanced detection sensitivity and specificity, the proposed sensor architecture incorporates a carefully engineered multilayer design, featuring bimetallic films composed of Ag and Au, in

combination with functional materials such as GaS and BF_4. A particularly noteworthy enhancement is introduced through the integration of few-layer BP, which significantly elevates the sensor's responsiveness to VOCs. This is largely attributed to BP's high surface reactivity and its effective interaction with gaseous analytes, especially those possessing exceptionally low refractive indices.

Furthermore, the optical characteristics of the sensor are rigorously analyzed by investigating the evanescent field distribution across the multilayered interface. This analysis provides deeper insight into the localized electric field behavior in the vicinity of the sensing surface, which is critical for optimizing sensor performance and ensuring reliable signal transduction. Together, these developments establish a robust foundation for next-generation VOC-based diagnostic tools in biomedical applications.

In contrast to previously reported SPR-based gas and biosensing platforms, the present study introduces a novel multilayer bimetallic SPR architecture specifically designed for non-invasive breath analysis targeting liver and pulmonary disease biomarkers. The proposed configuration uniquely integrates an Ag/Au bilayer with a phase-change GST layer and optimally stacked BP sheets to enhance light–matter interaction and electromagnetic field confinement at the sensing interface. Unlike earlier designs that primarily focused on sensitivity enhancement using individual 2D materials or single-metal films, this work systematically optimizes both material composition and layer thickness to maximize resonance angle shift for low-refractive-index VOC detection. Additionally, the study provides a detailed numerical investigation of evanescent field distribution and phase-dependent GST behavior, enabling tunable plasmonic response. The optimized sensor demonstrates significantly improved refractive index sensitivity for disease-specific VOC biomarkers, establishing a distinctive and application-oriented contribution toward high-performance, breath-based biomedical diagnostics. The illustration of the proposed framework is depicted in Fig. 1.

2 Methodology

In the present study, a SPR sensor employing the Kretschmann configuration is proposed and systematically analyzed as a high-performance optical sensing platform. The conceptual layout of the sensor architecture is illustrated in Fig. 2. The multilayered structure has been precisely engineered through the sequential deposition of functional materials, beginning with a NaF prism substrate, followed by layers of Ag, Au, GST, BP, and finally the analyte medium. To initiate SPW excitation at the metal-dielectric interface, a monochromatic, p-polarized light source with a wavelength of 632.8 nm is directed toward the sensor at varying angles of incidence. The resulting variation in reflectance is recorded by a photodetector strategically placed at the output to identify the resonance angle corresponding to SPW generation.

NaF is selected as the prism coupling medium due to its low refractive index (RI = 1.3245) and superior optical transparency across the visible spectrum. These characteristics make NaF an optimal candidate for efficient coupling of incident photons to plasmonic modes, thereby enhancing the sensitivity

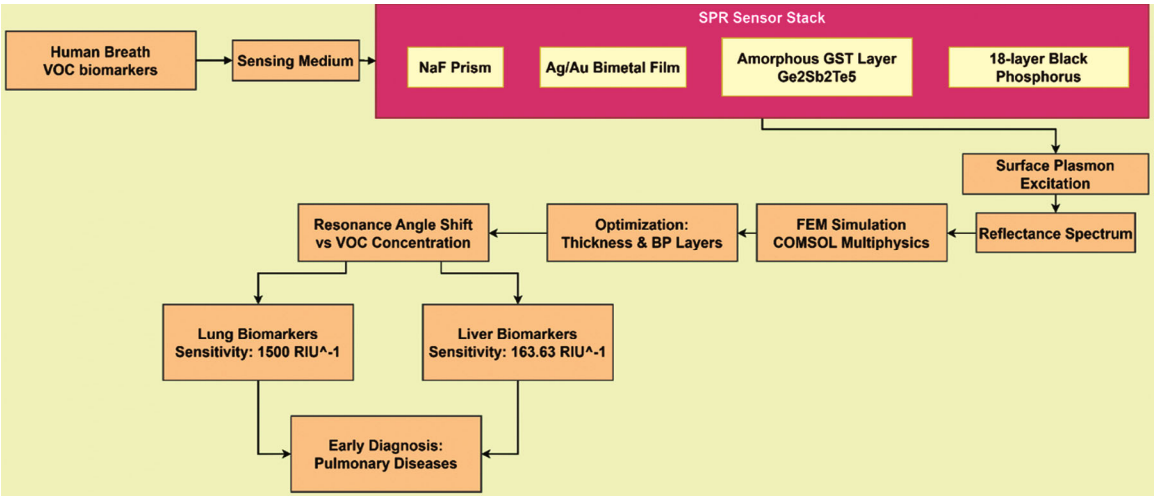

Fig. 1 — Proposed framework

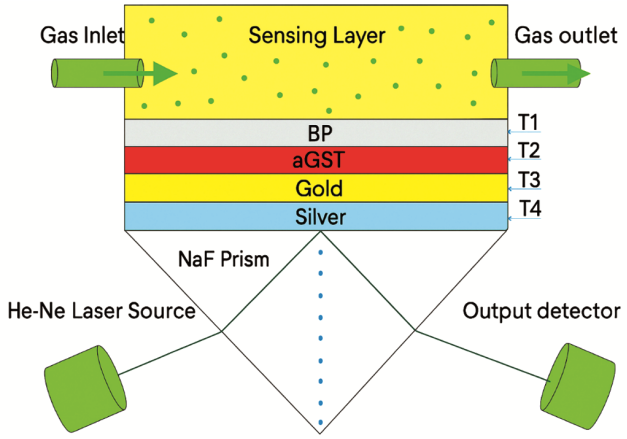

Fig. 2 — Conceptual design of the projected gas sensor

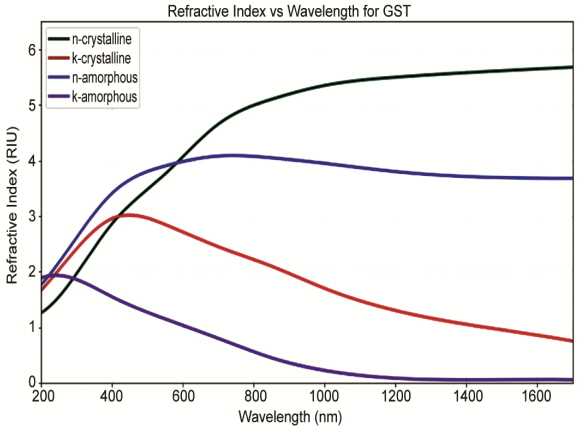

Fig. 3 — Wavelength dependent refractive index of GST phases

and resonance sharpness of the SPR sensor. This carefully tailored material configuration underpins the device's capability for precise analyte detection in complex sensing environments.

A NaF prism, exhibiting a complex RI of[28] 0.0803 + i4.2333, serves as the optical substrate and is overlaid with a Ag film to enable the excitation of SPR. Owing to its ability to produce sharp angular resonance features, Ag significantly improves the precision of detection. Nevertheless, due to its susceptibility to environmental degradation via oxidation, a protective Au layer is deposited atop the Ag, resulting in a bi-metallic structure. This Au coating not only enhances the chemical stability of the sensor but also contributes to improved sensitivity.

To further increase the optical absorption, a thin film of GST is incorporated into the structure. The GST layer is subsequently coated with BP, chosen for its exceptional potential in gas sensing due to its high surface reactivity and tunable electronic properties. The overall sensing performance is assessed by monitoring the angular displacement in reflectance corresponding to different concentrations (in parts per million).

The parameters λc and λp, which play a fundamental role in characterizing the optical behavior of the system. Figure 3 presents the experimentally acquired complex RI values of the GST material in its two distinct structural states—amorphous and crystalline as documented[10].

At the wavelength of 632.8 nm, the complex RI of the BP layer is reported to be 3.531 – 0.04087i, based on the findings[12]. An overview of the refractive indices and physical thicknesses of all the constituent layers incorporated into the sensor architecture is provided in Table 1.

Table 1 — Optical constants and layer thicknesses of selected materials

Layer No.	Material Name	λ = 633 nm		Thickness (nm)
		n	*k*	
1	Sodium Fluoride Prism	1.3260	0.0000	400
2	Silver	0.0825	4.2100	35
3	Gold	0.1415	3.5900	5
4	Amorphous GST	3.68	1.38	1.0
5	Black Phosphorus	3.540	–0.0425 *i*	L × 0.66
6	Sensing Medium	1.002 – 1.012	—	—

A rigorous examination of the reflectance spectra is essential to evaluate the operational performance of the SPR sensor. This analysis offers insight into the interplay between optical properties and sensor responsiveness. Among the critical performance metrics, sensitivity and FOM are of particular importance. Sensitivity is formally characterized by the degree of variation observed in the resonance angle when specific analyte molecules interact with and bind to the functionalized surface of the sensor. This angular shift serves as a measurable indicator of the sensor's responsiveness to target species, reflecting the efficiency and accuracy of the detection mechanism, as highlighted[8]. These parameters serve as foundational indicators for optimizing and benchmarking the efficiency of SPR-based sensing platforms.

To determine the RIs of metallic components such as Ag and Au, the wavelength-dependent Drude–Lorentz model is employed[6].

$$n_{metal}(\lambda) = \left(1 - \frac{\lambda^{*}\lambda_c}{\lambda^2 \; p(\lambda_c + i\lambda)}\right)^{\frac{1}{2}} \quad \ldots (1)$$

$$S\theta = \frac{\Delta\theta \text{ res}}{\Delta n} \quad \text{... (2)}$$

$$\text{FOM} = \frac{S\theta}{\text{FWHM}} \quad \text{... (3)}$$

Equations (1)–(3) collectively describe the optical modeling and performance evaluation framework of the proposed SPR sensor. Equation (1) characterizes the wavelength-dependent complex refractive index of the metallic layer, which governs surface plasmon excitation and resonance behavior. Equation (2) defines the angular sensitivity in terms of resonance angle shift with respect to refractive index variation, serving as the primary performance metric. Equation (3) further evaluates sensor quality through the figure of merit, incorporating both sensitivity and resonance sharpness to provide a comprehensive assessment of detection efficiency.

2.1 Fabrication

Figure 2 illustrates the sequential fabrication procedures involved in the development of the proposed SPR sensor. The fabrication process begins with the cleaning of the prism substrate using a piranha solution, typically composed of a mixture of sulfuric acid and hydrogen peroxide, to eliminate organic contaminants and ensure surface readiness.

Subsequently, bi-metallic layers of Ag and Au are deposited onto the cleaned prism using the PVD (Physical vapor deposition) technique. PVD encompasses three fundamental stages vaporization of the target material, its transport through a vacuum or controlled atmosphere, and subsequent condensation onto the substrate, enabling the formation of uniform thin films.

In the next step, active materials such as amorphous GST and BP are integrated onto the sensor structure. This can be achieved through CVD (Chemical vapor deposition) or, alternatively, by employing a chemical exfoliation method, depending on the desired material properties and deposition control.

To ensure precise assessment of the morphological characteristics, including the uniformity and thickness of the deposited thin films, FESEM (Field emission scanning electron microscopy) is utilized due to its high-resolution imaging capability. For the optical performance evaluation, an LED-based illumination system is employed, wherein the light is introduced from one end of the prism structure to facilitate angular reflectance measurements. The reflected optical signal is subsequently captured using a calibrated photodetector, which is interfaced with a computer system to enable automated spectral data acquisition. This configuration supports comprehensive analysis of the sensor's optical response by measuring reflectance, transmittance, and absorbance characteristics over the relevant spectral range[18].

3 Results and Discussion

The proposed sensor structure was subjected to rigorous numerical analysis using COMSOL Multiphysics, a finite element analysis platform specifically tailored for simulating multi-physics systems governed by mathematical equations. To accurately characterize the electromagnetic performance of the sensor, the EWFD (Electromagnetic Waves, Frequency Domain) module was utilized to numerically solve Maxwell's equations within the frequency domain framework. This computational approach enabled detailed simulation and analysis of the sensor's resonant characteristics, ensuring precise insight into its frequency-dependent behavior.

To maintain high simulation accuracy, especially in plasmonic regimes, the electromagnetic properties of the constituent materials most notably metals were defined with frequency-dependent complex permittivity and electrical conductivity parameters sourced from established experimental datasets. A customized meshing protocol was implemented to resolve nanoscale field variations effectively, with the mesh element size refined to range between 0.35 nm and 0.7 nm in regions proximal to metal-dielectric interfaces. Furthermore, PEC (Perfect Electric Conductor) boundary conditions were imposed on metallic boundaries to mimic ideal reflective surfaces and minimize numerical losses. The simulations were conducted using a frequency-domain solver to capture the system's spectral response and field distribution characteristics with high fidelity.

In order to realize the optimal operational performance of the proposed SPR sensor, meticulous optimization of the thickness parameters of its constituent material layers was performed. Among these, the metal layer exhibits significance, as its optical properties and physical thickness have a direct and pronounced effect on the sensor's key performance indicators. The interplay between these metrics governs the sharpness and depth of the

resonance curve, thereby influencing the precision and responsiveness of the sensor. Consequently, a careful balance between layer thickness and optical configuration is essential for maximizing the sensor's detection capability and overall efficiency in practical sensing environments.

In this study, systematic adjustments were made to both the metal and GST layers with the objective of minimizing reflectance. Within the SPR framework, RminRmin denotes the lowest reflectance point, which occurs when the resonance condition is precisely met by the incident light. This condition facilitates maximum excitation of SPs, leading to efficient energy transfer to the plasmonic mode.

Additionally, the sensor's sensitivity toward 2D materials was enhanced by modulating the BP layers. This adjustment allowed for effective interaction with analytes at the sensor interface. To ensure optimal resonance excitation, the entire multilayer structure was fine-tuned at a working wavelength of 632.8 nm, thereby ensuring accurate alignment with the SPR condition.

3.1 Structure Optimization

To facilitate a thorough and accurate assessment of the optical response of the sensor, a systematic analysis was conducted where in each individual material layer was examined in isolation. This approach was adopted to distinctly attribute the optical behavior to its respective constituent, thereby ensuring clarity in interpreting the sensor's overall performance. Figure 4 illustrates the angular dependence of reflectance for varying thicknesses of the Ag layer, which was incrementally adjusted in steps of 5 nm. This variation enabled a structured investigation into the impact of metallic layer thickness on the optical characteristics. The inset within the figure offers a magnified view of the evolution of the minimum reflectance values corresponding to different angles of incidence. This graphical representation highlights the sensitivity of the reflectance minima to variations in the Ag layer thickness, thus revealing its critical role in modulating the sensor's performance. The observed trends emphasize the necessity of optimizing layer dimensions to achieve enhanced sensitivity and tunability in optical sensing applications.

A detailed inspection of Fig. 5 reveals that a minimum reflectance of 4×10^{-3} a.u. is achieved when the Ag layer thickness is 35 nm. Consequently, this thickness is identified as the optimal value for enhancing the sensor's performance.

Figure 5 presents a detailed analysis of the angular variation in reflectance as a function of the gold layer thickness, systematically investigated in uniform steps of 5 nm. Throughout this analysis, the thickness of the underlying silver layer is held constant at 35 nm to isolate the influence of the gold layer on the optical response. This controlled variation allows for an isolated examination of the optical response attributed solely to the Au layer. The inset of Fig. 6 reveals a consistent and gradual increase in reflectance intensity corresponding to the progressive thickening of the Au layer. This observed enhancement indicates that increased Au thickness contributes positively to the overall optical reflectivity of the structure. Despite this trend, a trade-off exists between maximizing reflectance and minimizing resource consumption or potential optical losses due to excess material. Notably, the configuration employing a 5 nm Au layer exhibits a favorable balance between these competing considerations, offering sufficient reflectivity while

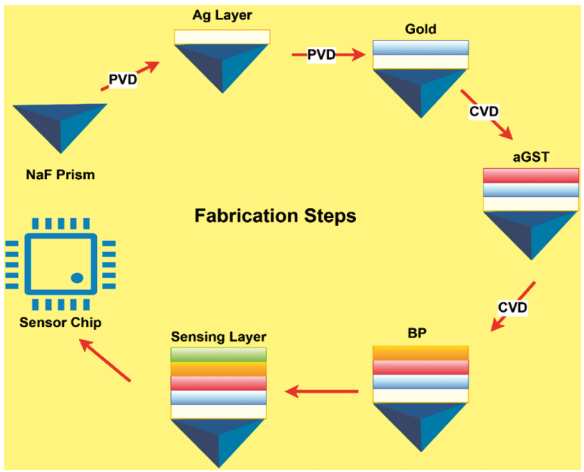

Fig. 4 — Systematic fabrication process of the sensor chip

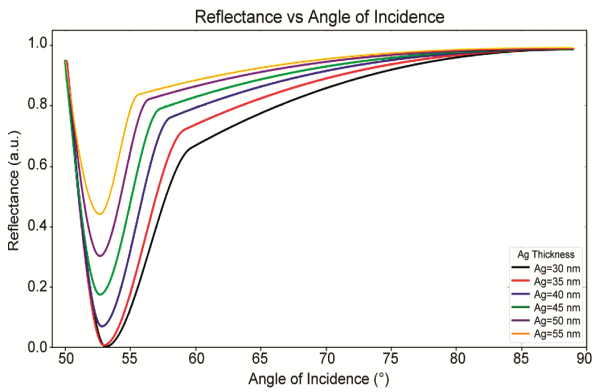

Fig. 5 — Effect of silver layer thickness on reflectance profile

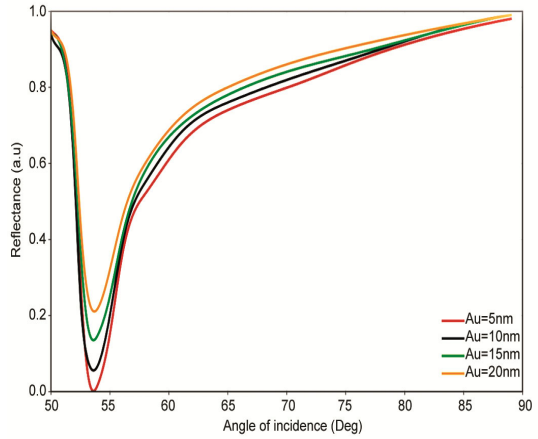

Fig. 6 — Effect of gold layer thickness on reflectance profile

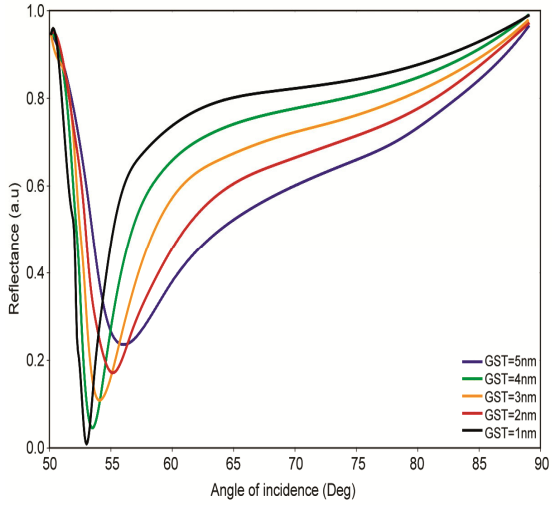

Fig. 7 — Effect of GST Layer thickness on reflectance profile

maintaining design efficiency. Based on this performance evaluation, the 5 nm Au layer is identified as the most effective thickness for subsequent stages of structural optimization and refinement within the design framework.

After finalizing the optimization of the metallic layer thickness, an in-depth investigation was undertaken to assess the impact of the GST layer on the sensor's optical performance characteristics. To identify the most effective GST thickness, the analysis commenced with an initial film of 1 nm, progressively increasing in uniform increments of 1 nm until reaching a maximum thickness of 7 nm. The simulation outcomes revealed a distinct trend: as the thickness of the GST layer increased, a noticeable broadening occurred in the SPR dip observed within the reflectance spectrum. This spectral broadening manifested as an increased FWHM (Full width at half

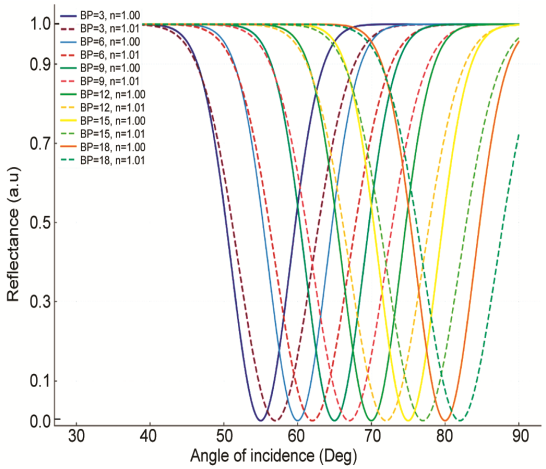

Fig. 8 — PR Response Curves with Varying BP Thickness (3L–18L) and Analyte Indices (n = 1.00, 1.01)

maximum) as depicted in Fig. 7. A higher FWHM typically signifies a degradation in the precision and sensitivity of the sensor, ultimately impairing its ability to detect minute refractive index changes effectively. Therefore, while the GST layer plays a critical role in modulating the device response, excessive thickness contributes to diminished performance due to reduced spectral sharpness and resolution. This finding highlights the necessity for careful control over the GST layer thickness to ensure optimal sensor functionality and maintain a high level of detection accuracy.

To enhance the sensitivity of the sensor and its capability to effectively capture bio-analytes, 2D materials were strategically integrated into its structural design. In particular, a thin layer of BP was deposited atop the GST layer, leveraging BP's remarkable surface affinity for gas molecule adsorption. The influence of BP on the sensor's optical response is illustrated in Fig. 8, which presents variations in the resonance angle. The solid curve represents the reflectance profile in the absence of gas analyte interaction (RI, n = 1), while the dotted curve corresponds to conditions following gas adsorption (n = 1.01). A noticeable shift in the resonance angle toward higher values is observed, along with a broadening of the reflectance curve both of which are indicative of enhanced analyte sensitivity and are depicted in the Fig. 8.

The phenomenon of resonance broadening observed in the sensor response can be primarily ascribed to the inherent dissipative or lossy nature of BP, a material known for its anisotropic optical and electrical characteristics. This material property enables efficient

absorption of the incident electric field, particularly at the interface formed between the BP layer and the adjacent analyte medium. Because of this absorption, there is a noticeable increase in the propagation constant associated with SPPs, thereby modifying the behavior of the resonance mode. The effect of varying L on the overall sensitivity of the plasmonic sensor configuration is systematically illustrated in Fig. 9. The graphical analysis shows that, as L increases, the sensor's angular sensitivity initially improves, reaching a maximum enhancement point of 189 degrees per RI unit (°/RIU) at L = 18. This improvement is attributed to the optimal balance between field confinement and plasmon damping provided by a suitable thickness of the BP layer. However, beyond this optimal threshold leads to a decline in sensitivity. This reduction is likely caused by excessive optical losses and limited field penetration, which collectively impair the efficient coupling between the SPW and the analyte, ultimately reducing the sensor's ability.

Additionally, the optimized sensor configuration was investigated using various metal combinations, including Cu and Al. Comparative analysis indicates that the structure comprising anAg and Au bilayer exhibits the highest sensitivity among the tested configurations. Thus, the Ag/Au combination is identified as the most effective metallic composition for enhancing SPR sensor performance. Table 2 summarizes the performance outcomes for each metal configuration evaluated in this study.

3.1 Detection of VOCs

The sensor's efficacy was evaluated through the detection of various VOCs present in dry exhaled breath. This assessment followed a rigorous optimization process focused on the thickness and layering of the constituent materials within the sensor architecture. In a healthy individual, the composition of dry exhaled breath typically comprises approximately 78% nitrogen, 5% carbon dioxide, 6% oxygen, and 1% other atmospheric gases, alongside trace concentrations of diverse VOCs.

Variations from established baseline concentrations of specific VOCs have been increasingly recognized as indicative of underlying pathological processes. Elevated levels of toluene have been associated with the progression of hepatic fibrosis, potentially due to its hepatotoxic effects and metabolic interference with liver function. Similarly, increased concentrations of isoprene, a naturally occurring endogenous VOC, have been linked to the early stages and progression

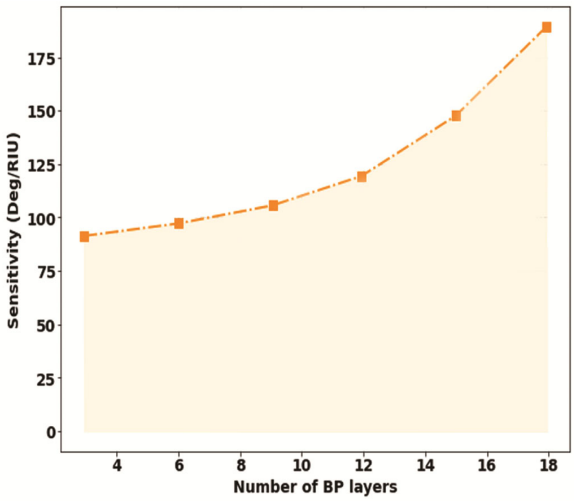

Fig. 9 — Effect of BP layer count on sensor sensitivity

Table 2 — Sensitivity analysis of various metal-based multilayer designs

S. No.	Layer Configuration					Sensitivity
	35nm	5 nm	1 nm	18L	Medium	
I	Ag	Au	GST	BP	Detection	192
II	Ag	Cu	GST	BP	Detection	178
III	Ag	Al	GST	BP	Detection	102

of pulmonary carcinogenesis, possibly reflecting alterations in lipid metabolism and oxidative stress associated with lung cancer pathophysiology[24, 26]. These findings underscore the emerging role of VOC profiling in medical diagnostics, offering promising avenues for the non-invasive detection, monitoring, and risk assessment of disease states[29].

Consequently, the analysis of exhaled breath serves as a valuable non-invasive biomarker for the early detection and diagnosis of pulmonary and hepatic diseases. To quantify the optical properties of isoprene and toluene within dry exhaled breath, the effective RI (n_eff) can be derived using the rule of mixtures, which is expressed as follows:

$$n_{eff} = \sqrt{\sum \quad in_i^2 V_i} \qquad \ldots (4)$$

Equation (4) defines the effective refractive index of the multilayer structure as a weighted contribution of the individual layer refractive indices based on their respective volume fractions.

The n_i values corresponding to individual gaseous components were referenced from established literature source[24]. Figures 10 and 11 illustrate the refractive index profiles of isoprene and toluene across varying concentration levels. Notably, both substances exhibit minimal refractive index variation

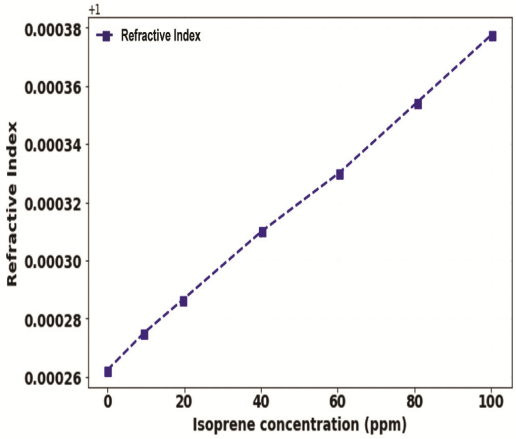

Fig. 10 — Variation of refractive index with isoprene concentration

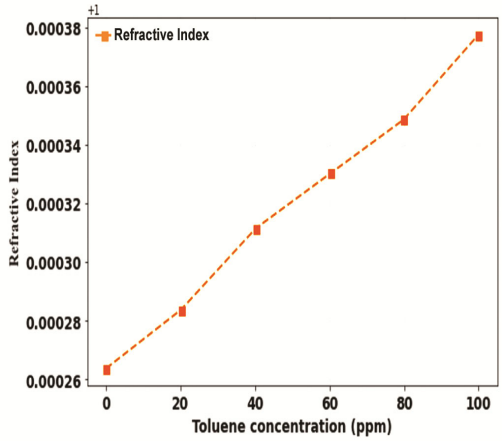

Fig. 11 — Variation of refractive index with toluene concentration

even with significant changes in concentration, thereby presenting a substantial challenge in their optical detection. This subtle variation emphasizes the indispensable requirement for a highly sensitive optical sensing platform that can reliably discern minute shifts in refractive index.

Figures 12 and 13 illustrate that the resonance angle undergoes a subtle shift corresponding to RI. This modest variation highlights the inherent challenges associated with detecting small differences in concentration. Furthermore, utilizing Eq. (3), the FOM was calculated for isoprene and for toluene, respectively. The ability to discern even minute fluctuations in VOC concentrations is critical for reliable sensing performance, and these results affirm the sensor's capacity to meet this requirement. The sensor's high sensitivity renders it particularly suitable for detecting subtle variations in isoprene and toluene levels, thereby supporting its potential application in precise gas monitoring systems.

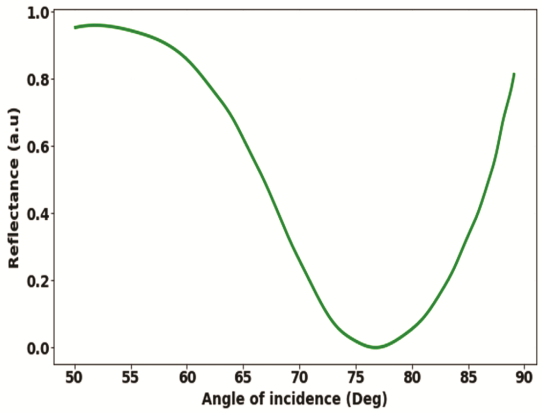

Fig. 12 — Reflectance as a function of angle of incidence for isoprene concentrations (0 ppm and 100 ppm)

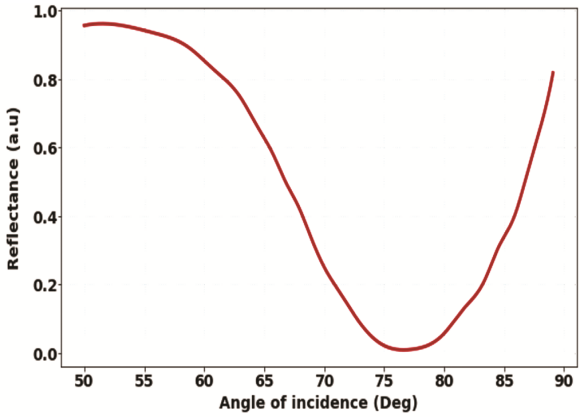

Fig. 13 — Reflectance as a function of angle of incidence for toluene concentrations (0 ppm and 100 ppm)

Notably, the detection of minor VOC concentration changes in exhaled breath offers valuable early indicators of diseases underscoring the sensor's significance in medical diagnostic contexts.

3.1 Electromagnetic Field Distribution in SPR Structures

The spatial characteristics of the electromagnetic field distribution in the SPR configuration are fundamentally important in determining the overall performance of the sensor. This distribution directly influences the extent of light–matter interaction at the interface, thereby controlling the sensor's sensitivity, signal strength, and ability to detect refractive index variations in the surrounding environment. A well-defined electric field localization near the sensing surface enhances resonance coupling and amplifies detection accuracy, making the analysis of field behavior essential for the design and optimization of high-performance SPR-based sensing systems. Under resonance conditions, a pronounced intensification of the electromagnetic field occurs, which is accompanied by a distinct dip in reflectance. This

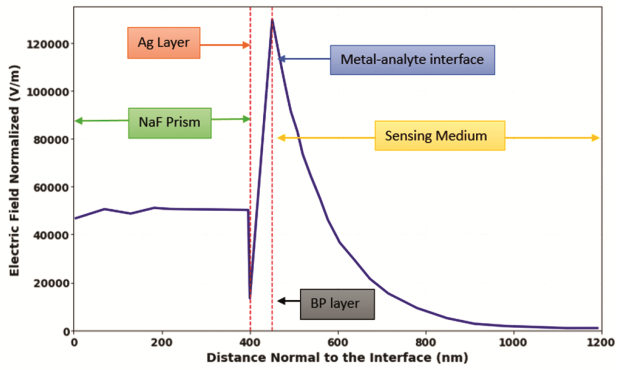

Fig. 14 — Electric field profile normal to the interface in BP–Ag–NaF–Analyte SPR structure

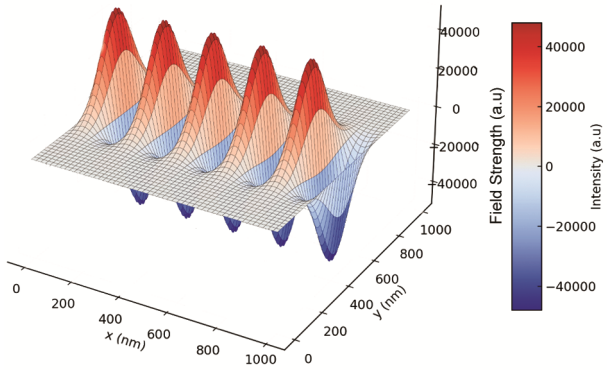

Fig. 15 — 3D Electric field distribution along the interface plane (XY-plane)

phenomenon leads to the efficient excitation of SPWs, resulting in the generation of an evanescent field that is strongly confined to the metal–dielectric interface. The intensity of this evanescent field reaches its peak at the interface and diminishes exponentially as it penetrates into the adjacent sensing medium. Owing to this steep spatial decay, the SPR mechanism exhibits heightened responsiveness to minor fluctuations in the RI immediately proximal to the metal–dielectric junction. Therefore, the sensor's performance is intimately tied to the magnitude and spatial confinement of the evanescent field, which directly influences its capacity to detect minute changes in the optical properties of the surrounding analyte environment[27].

Figure 14 presents the spatial distribution of the electric field across the multilayered sensor configuration, highlighting variations in field intensity at different interfacial boundaries. The electric field remains weak near the distal end of the coupling prism an area where SPR excitation does not occur indicating limited energy confinement. This enhanced field confinement highlights the sensor's capability to detect extremely subtle RI perturbations with heightened sensitivity. Furthermore, the penetration depth of the evanescent field was quantitatively assessed. This depth is characterized as the vertical distance within the sensing layer from the location of the peak electric field amplitude to the point where the amplitude diminishes to approximately 1/e (around 37%) of its maximum value. The calculated penetration depth for the proposed configuration is approximately 121.756 nm, indicating effective field extension into the sensing region, which is crucial for high-performance bio sensing applications.

In addition, Fig. 15 presents the 3-D spatial distributions, respectively, of the Ey component associated with the p-polarized electromagnetic field. These distributions are mapped across the multiple interfacial boundaries of the proposed multilayer sensor configuration, which is composed of sequential layers of Ag, Au, GST, BP (18 layers), and the sensing medium. The visual analysis clearly demonstrates that the incident p-polarized light effectively initiates the excitation of surface plasmon waves at the defined material interfaces. This excitation plays a pivotal role in enhancing the confinement of the electromagnetic field within the layered structure, which is essential for improving the sensing performance and optical sensitivity of the system.

As the evanescent electromagnetic field extends into the surrounding sensing domain, it facilitates efficient coupling with the target analyte, thereby intensifying the interaction at the interface and substantially enhancing the overall sensing performance. This mechanism is essential for detecting subtle changes in the local environment. Figure 16 illustrates the three-dimensional spatial distribution of the transverse electric field component (Ey), which clearly depicts the variation in field intensity and its propagation dynamics across the multilayered structural configuration. A pronounced field enhancement is observed specifically at the interface between the BP layer and the adjacent sensing medium. This localized amplification of the electric field plays a pivotal role in boosting the sensor's responsiveness to refractive index fluctuations. Such a pronounced sensitivity to dielectric perturbations is vital for ensuring high-precision detection, making the architecture particularly suitable for applications requiring accurate refractive index modulation monitoring.

The pronounced confinement and well-defined spatial distribution of the electric field within the proposed structure indicate its significant capability

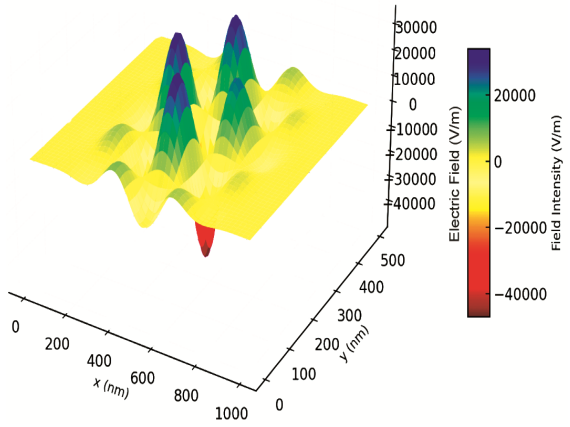

Fig. 16 — 3D Electric field intensity across the interface normal (XZ-plane)

Table 3 — Comparative evaluation with prior research outcomes

5	Structure					Sensitivity
[24]	Prism	Ag	BP	MoS_2	Air	112
[26]	Prism	Dual-metal	Dielectric	Dual-metal		70.1
[29]	Prism	Metal	BP	SM		125
Current Study	Prism	Ag	Au	a-GST	BP SM	192

for the accurate detection of subtle variations in refractive index. This enhanced sensitivity arises chiefly from the complex electromagnetic field dynamics that occur within the multilayered configuration, facilitating efficient light–matter interaction at the sensing interface. To validate the performance of the sensor, Table 3 presents a detailed comparative evaluation of its key metrics against those reported in recent peer-reviewed studies. The analysis highlights the superior performance of the proposed surface plasmon resonance configuration, thereby confirming its potential for high-precision sensing applications. The enhanced sensitivity of 192°/RIU arises from the synergistic integration of a bimetallic Ag/Au film, an amorphous GST layer, and optimized BP stacking, which collectively improve plasmon coupling, electromagnetic field confinement, and analyte interaction. This multilayer configuration significantly amplifies resonance angle shifts compared to previously reported single-metal BP-based structures (125°/RIU[29]).

4 Conclusion

This study presented a multilayer SPR sensor based on the Kretschmann configuration for the selective detection of VOC biomarkers in exhaled breath. The proposed architecture integrates a bimetallic Ag/Au layer, an amorphous GST film, and optimally stacked BP sheets to enhance plasmonic coupling and electromagnetic field confinement at the sensing interface. Finite element simulations were employed to analyze angular reflectance behavior and optimize structural parameters.

Compared with previously reported single-metal or limited multilayer SPR configurations, the proposed structure demonstrates a substantially enhanced sensitivity of 192°/RIU. This improvement is primarily attributed to three synergistic mechanisms: (i) reduced optical damping and stronger surface plasmon propagation enabled by the Ag/Au bilayer, (ii) refractive index modulation and enhanced field localization introduced by amorphous GST, and (iii) improved analyte interaction facilitated by multilayer BP. The optimized 18-layer BP configuration significantly strengthens the evanescent field intensity at the sensing boundary, resulting in larger resonance angle shifts for small refractive index variations.

Despite the improved performance, several practical considerations must be addressed for real-world implementation. The fabrication of uniform ultrathin GST and multilayer BP films requires precise deposition control and may introduce scalability challenges. Long-term material stability, especially for BP under ambient conditions, remains a critical factor. Furthermore, environmental cross-sensitivity and humidity effects in real breath samples may influence detection accuracy and require additional calibration strategies.

Overall, the proposed multilayer SPR platform offers a structurally efficient and high-sensitivity approach for breath-based biomarker detection. With further experimental validation and material stabilization strategies, the design holds strong potential for translation into practical, non-invasive biomedical diagnostic systems.

Future research should focus on experimental validation of the proposed multilayer SPR sensor to verify the simulated sensitivity under real operating conditions. Fabrication feasibility, thickness uniformity, and long-term stability of the Ag/Au–aGST–BP structure require systematic investigation, particularly considering the environmental sensitivity of black phosphorus. Benchmark testing using realistic breath mixtures containing clinically relevant concentrations of isoprene and toluene should be conducted to evaluate selectivity, cross-sensitivity, and robustness under varying humidity and temperature conditions. Additionally, future studies

should explore optimization through multi-parameter modeling and integration with portable optical interrogation systems to enable practical point-of-care diagnostic applications.

Appendix

Symbols	
Ag	Silver
Au	Gold
Al	Aluminum
Cu	Copper
NaF	Sodium Fluoride
Pt	Platinum
NO_2	Nitrogen dioxide
λc	Collision wavelengths
λp	Plasma wavelengths
L	The number of BP layers
n_i	Refractive index value
V_i	Volume fraction
n	Real part
k	Imaginary part

References

1 Nguyen H H, Park J, Kang S & Kim M, *Sensors*, 15 (5) (2015) 10481.
2 Then W L, Aguilar M I & Garnier G, *Sci Rep* 7 (1) (2017) 1616.
3 Chaudhary V S, Kumar D & Kumar S, *IEEE Trans Plasma Sci*, 49 (12) (2021) 3803.
4 Taya S A, Al-Ashi N E, Ramahi O M, Colak I & Amiri I S, *JOSA B*, 38 (8) (2021) 2362.
5 Agarwal S, Giri P, Prajapati Y K & Chakrabarti P, *IEEE Sens J*, 16 (24) (2016) 8865.
6 Pal S, Prajapati Y K & Saini J P, *Opt Rev*, 27 (1) (2020) 57.
7 Rahman M M, Abdulrazak L F, Ahsan M, Based M A, Rana M M, Anower M S & Gurusamy S, *IEEE Access*, 10 (2021) 689.
8 Wei K, Su X, Zheng J, Liu S, Chen B & Guo Y, *Optik*, 299 (2024) 171612.
9 Chauhan R, Saddeek Y, Kumari C, Sharma R C, Aly K A, Sharma P & Sharda S, *Phys B Condens Matter*, 713 (2025) 417364.
10 Almawgani A H M, Sorathiya V, Soni U, *et al*., *Plasmonics*, 20 (2025) 3505.
11 Almawgani A H M, Alhawari A R H, Sbeah Z, *et al.*, *Plasmonics,* 20 (7) (2025) 5433.
12 Katsidis C C & Siapkas D I, *Appl Opt*, 41 (19) (2002) 3978.
13 Singh M K, Pal S, Prajapati Y K & Saini J P, *IEEE Sens Lett*, 4 (7) (2020) 1.
14 Bao S, Li K, Ning P, Peng J, Jin X & Tang L, *Appl Surf Sci*, 393 (2017) 457.
15 Szunerits S, Maalouli N, Wijaya E, Vilcot J P & Boukherroub R, *Anal Bioanal Chem*, 405 (2013)1435.
16 Gan X, Zhao H & Quan X, *Biosens Bioelectron*, 89 (2017) 56.
17 Vasimalla Y & Pradhan H S, *Opt Quant Electron*, 54 (10) (2022) 612.
18 Maurya J B, Prajapati Y K, Raikwar S & Saini J P, *Optik*, 160 (2018) 428.
19 Almawgani A H M, Daher M G, Taya S A, *et al*., *Plasmonics,* 17 (2022) 1751.
20 Mohamed Ilyes H, Oualid D, Ghania H, *et al*., *Plasmonics,* 20 (2025) 9873.
21 Roy S, Mondol N, Kundu D, Meem A A, Islam M R, Hossain M A & Hossain M B, *Sens Bio-Sens Res,* 43 (2024) 100630.
22 Chen Y, Zhou R, Shu Y, Zhou H, Zheng W, Liu GL, Li Y & Huang L, *Biosens Bioelectron,* 287 (2025) 117740.
23 Karki B, Trabelsi Y, Sarkar P, Pal A & Uniyal A, *Mod Phys Lett B*, 39 (1) (2025) 2450364.
24 Popa C, Petrus M & Bratu A M, *J Biomed Opt*, 20 (5) (2015) 057006.
25 Karki B, Pal A, Sarkar P, Yadav R B, Muduli A & Trabelsi Y, *SILICON*, 16 (2024) 3861.
26 Hayton C, Terrington D, Wilson A M, Chaudhuri N, Leonard C & Fowler S J, *Respir Res*, 20 (1) (2019) 0971.
27 Shalabney A & Abdulhalim I, *Laser Photonics Rev*, 5 (4) (2011) 571.
28 Singh M K, Pal S & Prajapati Y K, *IEEE Trans Nano Biosci*, 22 (1) (2022) 106.
29 Dent A, Sutedja T & Zimmerman P, *J Thorac Dis*, 5 (5) (2013) 540.
30 Wulandani R, Milano V, Riswan M, Ramadhani R F, Anggraeni K, Jayanti P D, Istiqomah N I, Rini N P, Mahardhika L J, Darmawan M Y, Angel J & Suharyadi E, *Sensors Int*, 7 (2026) 100378.
31 Althuwayb A A, Rajan M S M, Alzaid M, Arun Kumar U & Hassan H M A, *Microchem J*, 221 (2026) 117030.
32 Kuiri B, Singh K, Biswas D, Kumar D, Gautam R K S G & Mondal R, *Ceram Int*, 52 (2) (2026) 2682.